Mineralogical Magazine (2024), **88**, 162–169
doi:10.1180/mgm.2023.91

Article

Immobilisation of chromium in magnesium carbonate minerals

Alicja M. Lacinska[1], Keith Bateman[1], Simon Chenery[1], Simon J Kemp[1], Thomas Liddy[2], Jeremy C Rushton[1], Dipankar Saha[3] and Sven L.M. Schroeder[3,4]

[1]British Geological Survey, Natural Environment Research Council, Environmental Science Centre, Keyworth, Nottingham NG12 5GG, UK; [2]The University of Nottingham, University Park Nottingham NG7 2RD, UK; [3]The University of Leeds, School of Chemical and Process Engineering, Leeds LS2 9JT, UK; and [4]Diamond Light Source Ltd, Harwell Science and Innovation Campus, Oxfordshire OX11 0DE, UK

Abstract

Hexavalent chromium (Cr^{6+}) is a toxic carcinogenic pollutant that might be released by the mining and processing of ultramafic rocks and nickel laterites and which requires permanent removal from the contaminated biosphere. Ultramafic material can also serve as a feedstock for the sequestration of CO_2 resulting from the growth of new minerals, raising the intriguing proposition of integrated sequestration of both pollutants, CO_2 and chromium, into magnesium carbonates. Such a synergistic process downstream of ore recovery and mineral processing could be an elegant proposition for more sustainable utilisation and management of the Earth's resources. We have therefore carried out an experimental and microanalytical study to investigate potentially suitable carbonate minerals. Uptake of chromium in carbonate phases was determined, followed by identification of the crystalline phases and characterisation of the local structural environment around the incorporated chromium centres. The results suggest that neither nesquehonite nor hydromagnesite have the structural capacity to incorporate Cr^{6+} or Cr^{3+} significantly at room temperature. We therefore propose that further research into this technology should focus on laboratory assessments of other phases, such as layered double hyroxides, that have a natural structural capacity to uptake both chromium and CO_2.

Keywords: hexavalent chromium; hydromagnesite; nesquehonite; ultramafics; laterites; environment; ore processing; carbon capture

(Received 3 July 2023; accepted 28 November 2023; Associate Editor: Juraj Majzlan)

Introduction

Decarbonising the world economy relies on a secure and sustainable supply of critical metals and minerals that underpin low-carbon technologies. The development of wind, hydro- and geothermal energy technologies, as well as energy storage systems and transport solutions with less environmental impact will continue to rely on primary mining for the foreseeable future, as more sustainable options, e.g. the recovery of metals from e-waste, cannot satisfy the demand for critical resources. However, although mining can bring numerous benefits to society and global economic development, almost all mining operations are associated with negative effects on the environment, including ecosystem loss and the heavy-metal pollution of water, soil, or dust. Mining is currently responsible for up to 7% of greenhouse-gas emissions globally (Delevingne *et al.*, 2020), of which emissions incurred directly through mining operations and power consumption make up ~1%. An additional 28% of global emissions are indirect and include coal-based power or gas combustion to process metals, and emissions generated upstream to produce mining equipment (Delevingne *et al.*, 2020).

Corresponding author: Alicja M. Lacinska; Email: alci@bgs.ac.uk
Cite this article: Lacinska A.M., Bateman K., Chenery S., Kemp S.J, Liddy T., Rushton J.C, Saha D. and Schroeder S.L.M. (2024) Immobilisation of chromium in magnesium carbonate minerals. *Mineralogical Magazine* **88**, 162–169. https://doi.org/10.1180/mgm.2023.91

The mitigation of greenhouse-gas emissions from mining operations can thus make a substantial contribution to climate change mitigation. This will require integration of clean energy technologies and carbon capture and storage (CCS) at different stages of the mining operation, from ore recovery to mineral processing. CCS can theoretically be achieved by either the injection of CO_2 *in situ* into suitable geological formations, where it can be immobilised by several mechanisms (Matter and Kelemen, 2009; Kelemen *et al.*, 2011; De Silva *et al.*, 2015) or by the reaction of CO_2 with feedstock materials to produce carbonate minerals. The latter is typically referred to as *ex situ* Carbon Capture and Storage by Mineralisation (CCSM). Recent advances in CCSM propose utilising carbonation as a metal recovery process (Wang *et al.*, 2021; Wang and Dreisinger, 2022, 2023). Some of the best feedstock materials for CCSM are magnesium (Mg)-rich ultramafic rocks, serpentinites and their weathering products (laterites). The last twenty years have seen significant progress in the understanding of mineralogical and geochemical factors controlling efficient carbonation (Zevenhoven *et al.*, 2003; Maroto-Valer *et al.*, 2005; Fagerlund *et al.*, 2009; Hanchen *et al.*, 2008; Fagerlund and Zevenhoven, 2011; Kelemen *et al.*, 2011; Werner *et al.*, 2013; Harrison *et al.*, 2013; Oskierski *et al.*, 2013; Power *et al.*, 2013; Lacinska *et al.*, 2016; Lacinska *et al.*, 2017; Power *et al.*, 2021), or the economic assessment of the technology (Strunge *et al.*, 2022) and CCSM is now advancing to pilot projects and medium-scale industrial

applications (MCi Carbon, 2023; Macpherson, 2023). In addition to their utilisation in CCSM, ultramafic rocks and laterites are also mined globally for battery and technology metals, such as nickel, cobalt and/or the platinum-group elements.

Conventional mining and processing of ultramafic rock-hosted ores is commonly associated with the generation and release of hexavalent chromium (Cr^{6+}), a toxic carcinogenic pollutant. The total Cr concentration in ultramafic rocks is estimated at 2 g/kg, approximately 10 times more than in mafic and 100 times more than in felsic rocks (Motzer, 2004). Chromium is redox sensitive and can adopt oxidation states ranging from −4 to +6. Trivalent and hexavalent chromium are the two most common naturally-occurring forms (Motzer, 2004). The trivalent species is mainly immobile in the environment and does not pose environmental risk, whereas the highly mobile Cr^{6+} is toxic in the biosphere when present at concentrations above the guideline value of 50 µg/L (World Health Organization, 2020).

The extent of water–rock interactions during the weathering of ultramafic rocks and serpentinites affects the concentration of Cr in the surrounding waters and soils, with the oxidation state dependent on the degree of redox reaction with other electron donors and acceptors present (McClain and Maher, 2016). For example, the occurrence of Cr^{6+} (~3–8% of the total chromium) in the lateritic regolith developed on ultramafic rocks in New Caledonia has been associated strongly with the presence of Mn^{3+} or Mn^{4+} (Fandeur *et al.*, 2009; Santos *et al.*, 2022). Notable amounts of Cr^{6+} found in natural systems have a direct anthropogenic origin, related to the sediment drainage from open pit mining (Gunkel-Grillon *et al.*, 2014) or pyro- and hydrometallurgical processing of ultramafic rocks and Ni laterites (PT Vale Indonesia Tbk, 2017).

Current Cr^{6+} remediation mechanisms include physical, chemical and/or biochemical processing of the waste materials. However, a recent review suggests that notwithstanding the significant capability of the various mechanisms, the associated cost, sustainability of the methods, sludge generation and huge amount of chemicals necessitate new innovative, environment-friendly propositions (Kumar and Dwivedi, 2021). An alternative process for Cr^{6+} remediation is to remove it through precipitation. This occurs naturally through reduction to Cr^{3+} and precipitation of insoluble Cr^{3+} oxides and hydroxides (Palmer, 1991). In naturally forming carbonates, the scavenging of potentially toxic elements (PTE), e.g. Cr, has been reported previously from travertines (Olsson *et al.*, 2014) and hydromagnesite (Boschi *et al.*, 2020). The pathway in which Cr can be incorporated crystallographically in minerals is determined primarily by its oxidation state. Trivalent Cr occupies the octahedral site of many minerals by substituting for Fe^{3+}, Al^{3+}, or Ti^{4+}. In contrast, Cr^{6+}, which is typically in the form of the chromate anion (CrO_4^{2-}), assumes tetrahedral coordination (Liu *et al.*, 2017). There are several naturally occurring minerals that contain both Cr^{3+} and carbonate ions in their crystal structures, including stichtite $Mg_6Cr_2CO_3(OH)_{16}{\cdot}4H_2O$ and grguricite $CaCr_2(CO_3)_2(OH)_4{\cdot}4H_2O$, however there are currently no known minerals with concurrent chromate and carbonate anions listed in the International Mineralogical Association database (Pasero, 2023). Such a combination is theoretically possible, albeit in actuality not yet reported, in layered double hydroxide or the ettringite-group minerals (Juroszek *et al.*, 2020). Hexavalent chromium has been reported from experimentally produced Ca carbonates, where chromate substitutes for the carbonate groups in calcite (Tang *et al.*, 2005; Hua *et al.*, 2007; Tang *et al.*, 2007; Sanchez-Pastor *et al.*, 2011). The incorporation mechanism requires overcoming a geometric incompatibility between the tetrahedral sites hosting Cr with the planar triangular carbonate groups causing local strain of the crystal structure (Tang *et al.*, 2007; Sanchez-Pastor *et al.*, 2011). Nevertheless, successful partitioning of Cr^{6+} into calcite has been observed, especially in strongly contaminated media, suggesting that the fate of this pollutant in natural environments can be influenced significantly by co-precipitation processes with carbonates (Sanchez-Pastor *et al.*, 2011).

Co-precipitation of chromium with magnesium carbonates has been less well studied, though nesquehonite ($MgCO_3{\cdot}3H_2O$) has been shown to incorporate Cr^{3+} through substitution with Mg^{2+} (Hamilton *et al.*, 2016; Hamilton *et al.*, 2018). Understanding the potential of Mg carbonates to trap chromium is of significant importance to mining and processing of ores hosted by ultramafic rocks. Here, we present an outlook on that potential based on experimental and microanalytical investigations.

Methodology

A series of co-precipitation experiments were conducted using aqueous solutions of $MgCl_2{\cdot}6H_2O$ (1.8 mol L^{-1}), $K_2Cr_2O_7$ (0.18 mol L^{-1}) and Na_2CO_3 (1.8 mol L^{-1}). Upon mixing at room temperature (20°C), the material became turbid immediately and a yellow gel formed. To monitor the speciation of chromate and its localisation in the resulting phases, a portion of the material was monitored continuously for eight hours by X-ray absorption near-edge structure (XANES) measurements during carbonate mineral crystallisation (Supplementary Fig. S1). A different portion of the same starting material was placed in an oven at 60°C for 6 hours, and XANES spectra were obtained subsequently. Additionally, an attempt to precipitate stichtite was made (Supplementary Figs S2 and S3), which resulted in poorly crystalline, albeit Cr-bearing, nano-scale particulates that are also the subject of investigation.

A multi-scale, multi-technique analytical programme was applied to elucidate the mineralogy and composition of the resulting materials, including overall material morphology by scanning electron microscopy (SEM), determination of crystalline phase composition by X-ray diffraction (XRD), element depth distribution profiles by energy-dispersive (EDX) X-ray analysis by SEM and laser-ablation inductively coupled plasma mass spectrometry (LA-ICP-MS) mapping. Determination of the chromium oxidation state and its local coordination environment in the crystal structure was achieved by XANES.

Scanning electron microscopy analyses were performed using a Zeiss Sigma 300 VP-FEG with Bruker Quantax XFlash 6|30 EDX detectors system at the British Geological Survey. Samples were analysed in the form of carbon sputter coated (≈25 nm thick) polished blocks and as rough materials distributed on an aluminium stub with carbon tab. The SEM was operated under conditions of high vacuum (1.2×10^{-6} Torr) at accelerating voltages ranging from 3–15 kV, with 8.5 mm optimal analytical working distance and an X-ray detector take-off angle of 35°. Qualitative compositional analyses of the mineral phases were performed using Bruker systems SDD EDS. Quantitative analysis was not undertaken due to analytical challenges associated with the fine grain size and beam sensitive nature of the experimental materials. High-resolution imagery was performed at low kV (3–5 kV) and using an in-lens secondary electron detector.

https://doi.org/10.1180/mgm.2023.91 Published online by Cambridge University Press

X-ray diffraction was performed using a Malvern PANalytical X'Pert Pro series X-ray diffractometer at the British Geological Survey, equipped with an X'Celerator detector, cobalt-target tube and generator operated at 45 kV and 40 mA, in Bragg-Brentano geometry. Samples for XRD were ground in an agate pestle and mortar and <10 mg subsamples mounted on silicon crystal 'zero background' substrates using a single drop of acetone. Diffraction data were analysed using Malvern PANalytical X'Pert *HighScore Plus version 5.1* software coupled to the 2022 version of the International Centre for Diffraction Data (ICDD) PDF4+ database (https://www.icdd.com/).

X-ray absorption near-edge structure (XANES) data were collected at the B18 beamline at the Diamond Light Source in Harwell, United Kingdom. The measurement conditions for reference data and the sample were the same. The Cr *K* XANES were recorded in fluorescence-yield mode with a 36-element solid-state Ge detector. A Si(111) double crystal monochromator was used, which provides an energy range from 4 to 11 keV (Dent *et al.*, 2009). The spectra were acquired in continuous scanning ('quick EXAFS', QEXAFS) mode from 5790 eV to 6630 eV with a step size of 0.25 eV. X-ray absorption spectroscopy (XAS) data analysis was performed using the *Demeter* software package (Ravel and Newville, 2005). Data were extracted using *WebPlotDigitizer* (Rohatgi, 2015).

Laser ablation inductively couple plasma mass spectrometry (LA-ICP-MS) analyses were done on polished blocks using Elemental Scientific Lasers imageGEO193 (British Geological Survey). For mapping these samples, the 193 nm excimer laser spot was a 10 × 10 µm square and the laser set to 20Hz repetition rate and a fluence of 4.4 J/cm^2; the beam was then rastered as a series of lines at 25 µm/s across the target area, all being controlled by the proprietary 'AV2' software. The ICP-MS was an Agilent 8900 series instrument controlled by *MassHunter* software, data were collected in a time resolved fashion for isotopes ^{23}Na, ^{24}Mg, ^{39}K, ^{42}Ca and ^{52}Cr with a dwell time of 14 ms except Cr with 35 ms. As well as the samples, standards SRM610 (NIST, USA) and GSD-1G (USGS, USA) were analysed as calibrants. All calibration calculations and mapping were performed using the Elemental Scientific Lasers *Iolite4* software taking the both the time resolved counts/s data from an Agilent file and the laser log file; for concentration calculation Mg was used as an internal standard with an assumed stoichiometric concentration of 288,000 mg/kg.

Results

The room-temperature (20°C) experiments with stirring resulted in the formation of prismatic crystals (<1 mm) of nesquehonite ($MgCO_3{\cdot}3H_2O$) and lesser amounts of hydromagnesite [$Mg_5(CO_3)_4(OH)_2{\cdot}4H_2O$] as spherules. Combined microbeam analyses on the nesquehonite crystals provided evidence that neither Cr^{6+} nor Cr^{3+} were incorporated into the structure of this mineral (Fig. 1a,e), however element-distribution maps did show Cr-bearing nano-scale particulates located at the surfaces of the main components (Fig. 1b). The surface particulates also contain Mg, Na, Cl and O though they were too fine grained for separation and further analysis to identify the phase.

The experiments at 60°C without stirring, resulted in the precipitation of spherical aggregates (<200 µm) of both hydromagnesite and dypingite, $Mg_5(CO_3)_4(OH)_2{\cdot}5H_2O$. Although no nesquehonite was detected by XRD or SEM analyses, trace amounts might be present. These spherules and the similarly sized spherules of hydromagnesite from the 20°C precipitation are shown in Fig. 1d and 1c, respectively.

Microbeam raster analyses and compositional mapping of hydromagnesite (20°C experiment) revealed a notable (6–8 g/kg) association of chromium with the spherulite cores, commonly seen with Na and/or Cl, probably originating from halite (NaCl) and/or other nano-sized phases, interspersed and/or intergrown with the hydromagnesite (Fig. 1f). The distribution of chromium in hydromagnesite–dypingite (60°C) is notably different and comprises a more even dispersion of the element across a whole spherulite, with the highest concentration observed consistently in the marginal zones of increased microporosity (Fig. 1g). The amount of chromium associated with the spherulites formed at 60°C is an order of magnitude lower than in the precipitates from the 20°C experiment.

X-ray absorption near-edge structure (XANES) at the Cr *K*-edge collected from the hydromagnesite spherulites (20°C) shows a prominent pre-edge peak at 5995.5 eV, indicating the presence of Cr^{6+}, whereas the Cr *K* XANES pre-edge of hydromagnesite/dypingite formed at 60°C contains only two weak peaks at 6010 eV and 6025 eV, which are indicative of Cr^{3+} (Fig. 2b). The presence of Cr^{3+} is probably the result of chromium reduction during or after the precipitation. The exact molecular-level mechanism for this reduction and its timing are currently unclear. One possible mechanism might involve the ubiquitous chlorine present in the experiment, the redox reactions accompanying the oxidation of the chloride ion and the reduction of chromium to Cr^{3+} in the solution. The processes are complex and proceed *via* several intermediates, however they could lead to the formation of chlorine gas (and temperature driven evaporation) and/or chlorate (ClO_3^-) catalysed by the presence of chromate (CrO_4^{2-}) (Busch *et al.*, 2022). As no reduction occurred during the 20°C experiment, we can exclude radiolytic reduction by the X-ray beam. The increase of temperature to 60°C appears to be the trigger of the reactions. Indeed, previous *in situ* XANES of Cr $(OH)_3$ revealed strongly temperature-dependent interconversions between Cr^{3+} and Cr^{6+} (Schroeder *et al.*, 1997). This dependence of speciation on the process conditions may be potentially important in the long-term design of industrial crystallographic trapping of Cr in the carbonate structure and deserves further investigation.

However, if chloride–chromate redox reactions have occurred, then we speculate the following set of events resulted in the lower concentration and a more even distribution of chromium as Cr^{3+} in the spherulites that formed at 60°C: (1) rapid trapping of Cr^{6+} in amorphous magnesium carbonate (AMC); (2) reduction of the residual Cr^{6+} in the solution to Cr^{3+}, driven by reactions involving chloride and/or temperature-dependent interconversion between chromium species, and precipitation as $Cr(OH)_3$; which (3) creates a chromium concentration gradient between the solid and the solution, which in turn drives the diffusion of Cr^{6+} trapped in the solid out to the solution phase. Diffused chromium undergoes reduction and precipitation, as per (2), until the cessation of the 6 hours experiment.

The higher concentration of chromium in the outer zones of the spherulites (Fig. 1g) might have resulted from a combination of: (1) diffusion of core zone chromium towards the margin and reduction upon contact with solution; and (2) reduction of *in situ* chromium, with the width of the chromium-rich rim representing the depth of chloride-bearing solution penetration into the solid. Regardless, it is apparent that the diffused and *in situ* chromium have been mostly expelled from the solid upon the crystallisation of AMC into hydromagnesite/dypingite. Further trace-element investigations are needed to establish if any chromium was

https://doi.org/10.1180/mgm.2023.91 Published online by Cambridge University Press

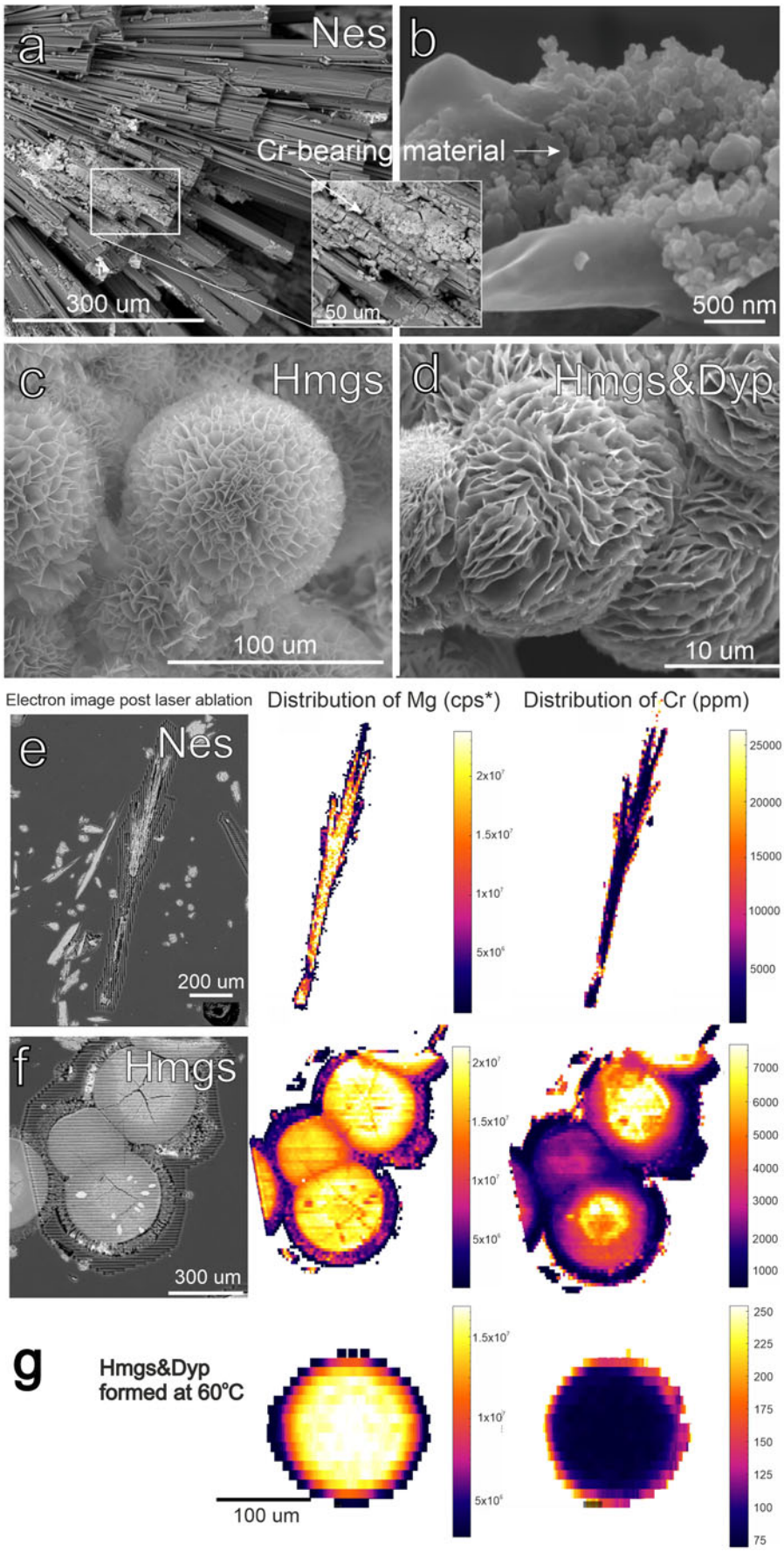

Figure 1. Secondary electron images of (a) prismatic crystals of nesquehonite locally covered by nano-sized Cr-bearing material, shown in detail in (b); (c) spherulites of hydromagnesite formed at 20°C and (d) hydromagnesite/dypingite formed at 60°C; (e) back-scattered electron and LA-ICP-MS maps showing the distribution of Mg and Cr nesquehonite prismatic crystals; (f) back-scattered electron and LA-ICP-MS maps showing the distribution of Mg and Cr in the hydromagnesite, 20°C; (g) LA-ICP-MS maps showing the distribution of Mg and Cr in the 60°C precipitates. Note: Mg is shown in cps as it was used as an internal standard.

https://doi.org/10.1180/mgm.2023.91 Published online by Cambridge University Press

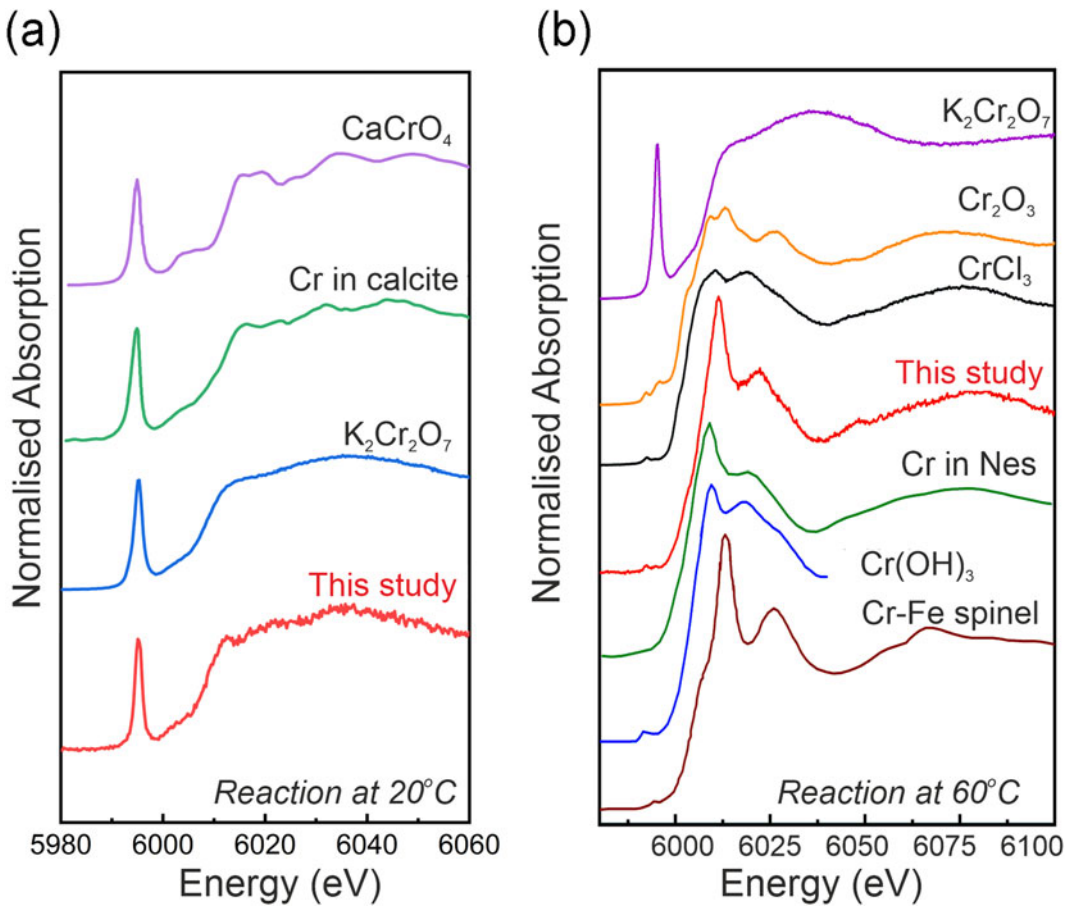

Figure 2. (a) Cr *K*-edge XANES spectra, with the 5995.5 eV Cr^{6+} pre-edge peak, collected from isolated spherulites of hydromagnesite formed at 20°C (in red – this study), $K_2Cr_2O_7$, $CaCrO_4$ (Tang *et al.*, 2007) and Cr-doped calcite (c25-1hr from Tang *et al.*, 2007). (b) XANES of hydromagnesite/dypingite spherulites formed at 60°C (in red – this study), compared to Cr^{3+}-bearing reference materials, including Cr in nesquehonite (Nes) (Hamilton *et al.*, 2016) and $K_2Cr_2O_7$, i.e. the initial host of chromium.

captured crystallographically, and if so, what the effect of such structural substitution is on the stability of the carbonate mineral.

Discussion and outlook

On the basis of the rapid precipitation of carbonate (seconds) in the static experiment and the spherical morphology and texture of hydromagnesite and dypingite, we infer that the initial material formed was amorphous and attained crystalline structure over time. Nesquehonite was the predominant phase identified in the stirred experiments. Such dynamic systems are known to promote the transformation of amorphous magnesium carbonate in aqueous solution to long-range ordered minerals, such as nesquehonite (Yamamoto *et al.*, 2021).

Our current understanding of the striking, albeit inconsistent association of Cr^{6+} with the cores of hydromagnesite spherulites does not support a structural incorporation mechanism, instead it suggests a physical trapping of Cr-bearing material in the intercrystalline microporosity of the aggregates (Fig. 3). The coexistence of and, the notably more even distribution of Cr^{3+} within hydromagnesite–dypingite spherical aggregates formed at 60°C, in addition to the similarity of our XANES data with that of Cr $(OH)_3$, are intriguing (Fig. 2) and suggest the potential incorporation of hydroxide. Trivalent chromium might be incorporated into carbonate as shown by previous investigations (Hamilton *et al.*, 2016; Boschi *et al.*, 2020) although not necessarily by a direct Cr^{3+} to Mg^{2+} substitution. In calcium carbonate, Cr^{3+} cannot substitute directly for Ca^{2+}, however as hydroxide, it may be adsorbed to crystal surfaces or occupy interstitial voids in the crystals (Fang *et al.*, 2022). A similar phenomenon might be true for magnesium carbonates (Fig. 3), and in such cases, chromium would have been expelled from the carbonate structure during the crystallisation of AMC. The crystallisation of AMC and the degree to which incompatible elements are incorporated structurally or physically, and/or expelled from the crystalline material might depend on the mechanism of crystallisation, i.e. dissolution–reprecipitation *versus* solid-state crystallisation. In the latter, a cascade of fast exchanges of hydrogen between the AMC and H_2O molecules from the hydration shell and the surrounding solution, enhances mobility of ions/molecules that compose the AMC (Von Euw *et al*, 2020). This allows for the rearrangement of AMC into crystalline domains *via* solid-state transformation (*idem*), possibly promoting the expulsion of incompatible elements and their physical entrapment in the local microporosity, as observed in the spherulites formed in this investigation. Although the spherulite morphology of hydromagnesite–dypingite precipitates is consistent with solid-state crystallisation, the dissolution–reprecipitation mechanism or a combination of both crystallisation pathways can not be ignored. Dissolution–reprecipitation would probably remove incompatible

https://doi.org/10.1180/mgm.2023.91 Published online by Cambridge University Press

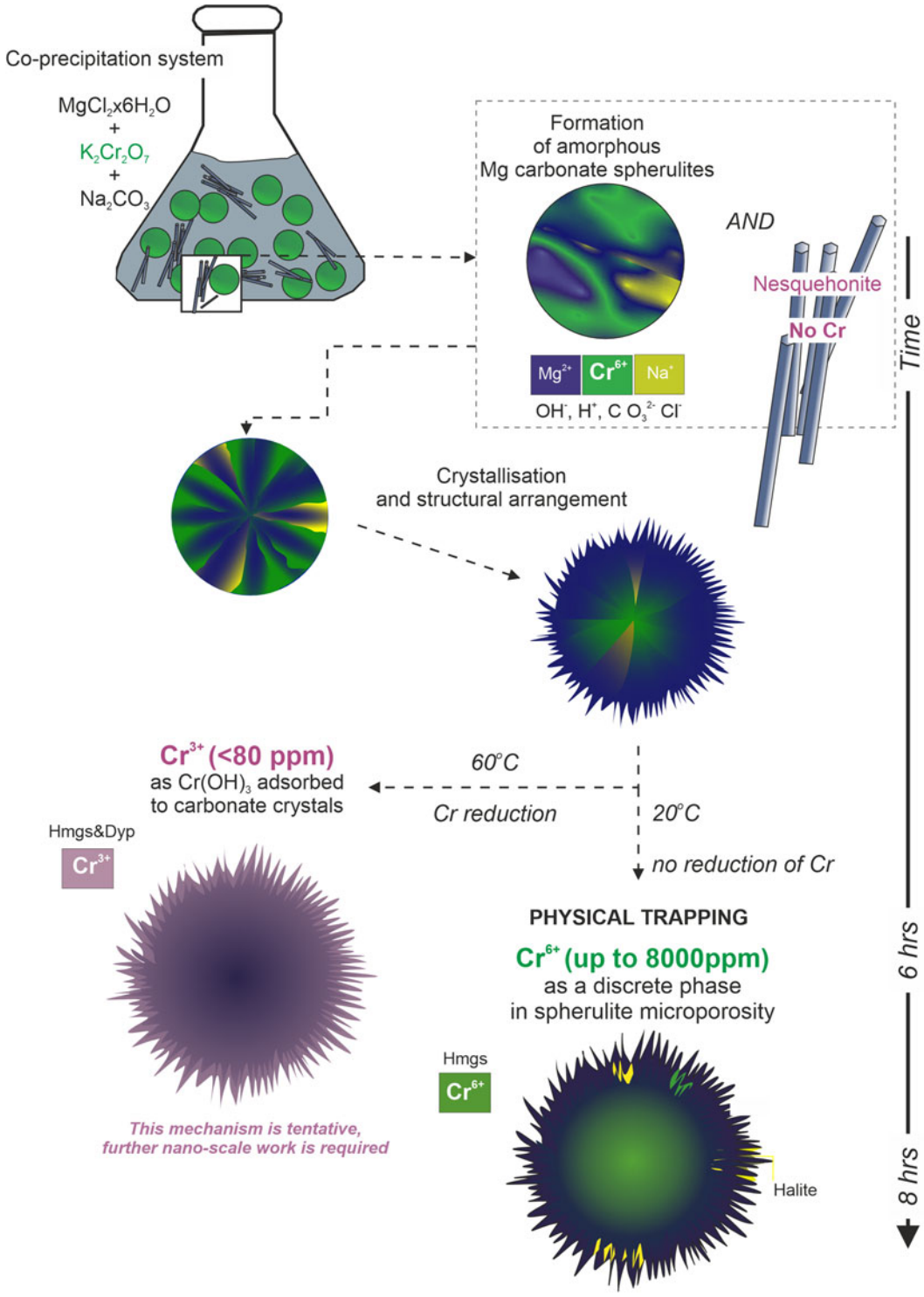

Figure 3. Possible incorporation mechanisms of chromium in Mg carbonates, including physical trapping and adsorption.

elements from the vicinity of the crystallising solid into the solution, decreasing the degree of entrapment and ultimately leading to the release of these elements. The phase-transformation mechanisms, including both the AMC to crystalline and subsequent changes to crystal structure within the hydrated–anhydrous magnesium carbonate system, are highly relevant to the cycling of potential contaminants such as chromium (Harison *et al*, 2019). Further experimental and nanoscale investigations are required to appraise the incorporation mechanism in detail. One potential avenue to explore is pressure-induced crystallisation that has been shown as an efficient pathway to dope incompatible elements into crystals of calcium carbonates (Matsunuma *et al.*, 2014).

In our opinion, experimental efforts should also focus on such Cr^{3+}-bearing materials that have a natural long-term capacity to retain chromium, rather than forcing structure-modifying

https://doi.org/10.1180/mgm.2023.91 Published online by Cambridge University Press

incompatible chromate ions into an otherwise stable structure of magnesium carbonates. Accordingly, we recognise that minerals belonging to the layered double hydroxides (LDHs), specifically the CO_2-bearing hydrotalcite supergroup with pyroaurite–hydrotalcite–stichtite end-members might present a viable matrix for chromium. These minerals comprise positively charged brucite-like layers $(A_{6-x}B_{2+x})(OH)_2$, where A is a divalent cation (e.g. Mg or Fe) and B is a trivalent cation (e.g. Al, Fe or Cr). Interlayer regions typically contain a monovalent or divalent anion X, such as CO_3^{2-}, SO_4^{2-}, Cl^- and OH^-. The well-defined structural site for trivalent elements and the wide range of possible cation–anion substitutions suggest that hydrotalcites represent a potentially suitable matrix for chromium or other PTE and CO_2 (Aschenbrenner *et al.*, 2011). Although the incorporation of trivalent chromium in hydrotalcite is relatively straightforward, albeit requiring metal reduction, the substitution of chromate for carbonate is challenging because of structural affinity of the CO_3^{2-} ion to the local symmetry of the interlayer site in hydrotalcite and the strong hydrogen bonding between the hydroxyl ions of the layer with the carbonate ions (Prasanna and Kamath, 2008). This makes the CO_2-bearing hydrotalcite very stable and thus it has a wide range of applications, including the cement industry (Bernard *et al.*, 2022). The hydrotalcite supergroup with pyroaurite–hydrotalcite–stichtite end-members represents a potential stable host for chromium and the CO_2 formed through integrated CCSM.

We, thus hypothesise that a disruptive innovation in the design of Ni laterite ore processing to include CO_2 and chromium sequestration through the precipitation of hydrotalcite will lead to more sustainable utilisation and management of the Earth's resources. Such process integration necessitates knowledge cross-fertilisation and a shared vision between industry and academia to timely assess its potential and drive the theory of change in the ore processing industry.

Acknowledgements. The research was part of the BGS International NC programme 'Geoscience to tackle Global Environmental Challenges', NERC reference NE/X006255/1. The authors publish with the permission of the Executive Director of the British Geological Survey (UKRI). Dr Michael Styles and Dr Kathryn Goodenough are acknowledged for providing an internal review of the manuscript. DS and SLMS acknowledge financial support by EPSRC through the Future Continuous Manufacturing and Advanced Crystallisation (CMAC) Hub (EP/P006965/1). DS was financially supported by Innovate UK under a Knowledge Transfer Partnership. We acknowledge the allocation of B18 beamtime by Diamond Light Source under the reference SP28772-1 and thank the beamline scientists Diego Gianolio and Veronica Cellorio for their support. John Fletcher (BGS) is thanked for the preparation of polished blocks for microanalysis. The authors thank anonymous reviewers and the editors of the journals for their valuable comments that improved the quality of the paper. All data supporting this study are provided either in the results section of this paper or in the electronic supplementary information accompanying it.

Supplementary material. The supplementary material for this article can be found at https://doi.org/10.1180/mgm.2023.91.

Competing interests. The authors declare none.

References

Aschenbrenner O., McGuire P., Alsamaq S., Wang J.W., Supasitmongkol S., Al-Duri B., Styring P. and Wood J. (2011) Adsorption of carbon dioxide on hydrotalcite-like compounds of different compositions. *Chemical Engineering Research & Design*, **89**, 1711–1721.

Bernard E., Zucha W.J., Lothenbach B. and Mader U. (2022) Stability of hydrotalcite (Mg-Al layered double hydroxide) in presence of different anions. *Cement and Concrete Research*, **152**, 106674.

Boschi C., Bedini F., Baneschi I., Rielli A., Baumgartner L., Perchiazzi N., Ulyanov A., Zanchetta G. and Dini A. (2020) Spontaneous serpentine carbonation controlled by underground dynamic microclimate at the Montecastelli copper mine, Italy. *Minerals*, **10**, https://doi.org/10.3390/min10010001

Busch M., Simic N. and Ahlberg E. (2022) Exploring the mechanism of Cr(VI) catalyzed hypochlorous acid decomposition. *Chemcatchem*, **14**, e202101850.

Delevingne L., Glazener W. Grégoir L. and Henderson K. (2020) *Climate Risk And Decarbonization: What Every Mining CEO Needs To Know*. McKinsey & Company. Online article: https://www.mckinsey.com/capabilities/sustainability/our-insights/climate-risk-and-decarbonization-what-every-mining-ceo-needs-to-know.

Dent A.J., Cibin G., Ramos S., Smith A.D., Scott S.M., Varandas L., Pearson M.R., Krumpa N.A., Jones C.P. and Robbins P.E. (2009) B18: A core XAS spectroscopy beamline for Diamond. *Journal of Physics: Conference Series*, **190**, 012039.

De Silva G.P.D., Ranjith P.G. and Perera M.S.A. (2015) Geochemical aspects of CO_2 sequestration in deep saline aquifers: A review. *Fuel*, **155**, 128–143.

Fagerlund J. and Zevenhoven R. (2011) An experimental study of $Mg(OH)_2$ carbonation. *International Journal of Greenhouse Gas Control*, **5**, 1406–1412.

Fagerlund J., Teir S., Nduagu E. and Zevenhoven R. (2009) Carbonation of magnesium silicate mineral using a pressurised gas/solid process. *Energy Procedia*, 1, 4907–4914 [Proceedings of the 9th International Conference on Greenhouse Gas Control Technologies, November 2008, Washington, DC.]

Fandeur D., Juillot F., Morin G., Olivi L., Cognigni A., Webb S.M., Ambrosi J.P., Fritsch E., Guyot F. and Brown G.E. (2009) Xanes evidence for oxidation of Cr(III) to Cr(VI) by Mn-oxides in a lateritic regolith developed on serpentinized ultramafic rocks of New Caledonia. *Environmental Science & Technology*, **43**, 7384–7390.

Fang Z.Y., Liu W., Yao T., Zhou G.T., Wei S.Q. and Qin L.P. (2022) Experimental study of chromium (III) coprecipitation with calcium carbonate. *Geochimica Et Cosmochimica Acta*, **322**, 94–108.

Gunkel-Grillon P., Laporte-Magoni C., Lemestre M. and Bazire N. (2014) Toxic chromium release from nickel mining sediments in surface waters, New Caledonia. *Environmental Chemistry Letters*, **12**, 511–516.

Hamilton J.L., Wilson S.A., Morgan B., Turvey C.C., Paterson D.J., MacRae C., McCutcheon J. and Southam G. (2016) Nesquehonite sequesters transition metals and CO_2 during accelerated carbon mineralisation. *International Journal of Greenhouse Gas Control*, **55**, 73–81.

Hamilton J.L., Wilson S.A., Morgan B., Turvey C.C., Paterson D.J., Jowitt S.M., McCutcheon J. and Southam G. (2018) Fate of transition metals during passive carbonation of ultramafic mine tailings via air capture with potential for metal resource recovery. *International Journal of Greenhouse Gas Control*, **71**, 155–167.

Hanchen M., Prigiobbe V., Baciocchi R. and Mazzotti M. (2008) Precipitation in the Mg-carbonate system - effects of temperature and CO_2 pressure. *Chemical Engineering Science*, **63**, 1012–1028.

Harrison A.L., Power I.M. and Dipple G.M. (2013) Accelerated carbonation of brucite in mine tailings for carbon sequestration. *Environmental Science & Technology*, **47**, 126–134.

Harrison A.L., Mavromatis V., Oelkers E.H. and Bénézeth P. (2019) Solubility of the hydrated Mg-carbonates nesquehonite and dypingite from 5 to 35°C: Implications for CO_2 storage and the relative stability of Mg-carbonates. *Chemical Geology*, **504**, 123–135.

Hua B., Deng B.L., Thornton E.C., Yang J. and Amonette J.E. (2007) Incorporation of chromate into calcium carbonate structure during coprecipitation. *Water Air and Soil Pollution*, **179**, 381–390.

Juroszek R., Kruger B., Galuskina I., Kruger H., Vapnik Y. and Galuskin E. (2020) Siwaqaite, $Ca_6Al_2(CrO_4)_3(OH)_{12}\times26H_2O$, a new mineral of the ettringite group from the pyrometamorphic Daba-siwaqa complex, Jordan. *American Mineralogist*, **105**, 409–421.

Kelemen P.B., Matter J., Streit E.E., Rudge J.F., Curry W.B. and Blusztajn J. (2011) Rates and mechanisms of mineral carbonation in peridotite: Natural processes and recipes for enhanced, in situ CO_2 capture and storage. Pp. 545–576 in: *Annual Review of Earth and Planetary Sciences* (R. Jeanloz and K.H. Freeman, editors), volume 39.

Kumar V. and Dwivedi S.K. (2021) A review on accessible techniques for removal of hexavalent chromium and divalent nickel from industrial wastewater: Recent research and future outlook. *Journal of Cleaner Production*, **295**, 126229.

Lacinska A.M., Styles M.T., Bateman K., Wagner D., Hall M.R., Gowing C. and Brown P.D. (2016) Acid-dissolution of antigorite, chrysotile and lizardite for ex situ carbon capture and storage by mineralisation. *Chemical Geology*, **437**, 153–169.

Lacinska A.M., Styles M.T., Bateman K., Hall M. and Brown P.D. (2017) An experimental study of the carbonation of serpentinite and partially serpentinised peridotites. *Frontiers in Earth Science*, **5**, https://doi.org/10.3389/feart.2017.00037.

Liu C., Hystad G., Golden J.J., Hummer D.R., Downs R.T., Morrison S.M., Ralph J.P. and Hazen R.M. (2017) Chromium mineral ecology. *American Mineralogist*, **102**, 612–619.

Macpherson A. (2023) *Researchers discover a way to improve mining yields while capturing CO_2 from the atmosphere*. University of Alberta, USA. Online article, https://www.ualberta.ca/folio/2023/04/researchers-discover-way-to-improve-mining-yields-while-capturing-co2.html.

Maroto-Valer M.M., Fauth D.J., Kuchta M.E., Zhang Y. and Andresen J.M. (2005) Activation of magnesium rich minerals as carbonation feedstock materials for CO_2 sequestration. *Fuel Processing Technology*, **86**, 1627–1645.

Matsunuma S., Kaqi H., Komatsu K., Maruyama K. and Yoshino T. (2014) Doping incompatible elements into calcite through amorphous calcium carbonate. *Crystal Growth & Design*, **14**, 5344–5348.

Matter J.M. and Kelemen P.B. (2009) Permanent storage of carbon dioxide in geological reservoirs by mineral carbonation. *Nature Geoscience*, **2**, 837–841.

McClain C.N. and Maher K. (2016) Chromium fluxes and speciation in ultramafic catchments and global rivers. *Chemical Geology*, **426**, 135–157.

MCi Carbon (2023) *MCi Carbon*. https://www.mineralcarbonation.com/.

Motzer W.E.A.E. (2004) Chemistry, geochemistry, and geology of chromium and chromium compounds. Chapter 2 in: *Chromium (VI) Handbook*. 1st Edition. Taylor Francis, Boca Raton, USA.

Olsson J., Stipp S.L.S. and Gislason S.R. (2014) Element scavenging by recently formed travertine deposits in the alkaline springs from the Oman Semail ophiolite. *Mineralogical Magazine*, **78**, 1479–1490.

Oskierski H.C., Dlugogorski B.Z. and Jacobsen G. (2013) Sequestration of atmospheric CO_2 in chrysotile mine tailings of the Woodsreef asbestos mine, Australia: Quantitative mineralogy, isotopic fingerprinting and carbonation rates. *Chemical Geology*, **358**, 156–169.

Palmer C.D. and Wittbrodt P.R. (1991) Processes affecting the remediation of chromium-contaminated sites. *Environmental Health Perspective*, **92**, 25–40.

Pasero M. (2023) *The New IMA List of Minerals*. International Mineralogical Association. Commission on new minerals, nomenclature and classification (IMA-CNMNC). http://cnmnc.units.it/.

Power I.M., Wilson S.A. and Dipple G.M. (2013) Serpentinite carbonation for CO_2 sequestration. *Elements*, **9**, 115–121.

Power I.M., Paulo C., Long H.N., Lockhart J.A., Stubbs A.R., French D. and Caldwell R. (2021) Carbonation, cementation, and stabilization of ultramafic mine tailings. *Environmental Science & Technology*, **55**, 10056–10066.

Prasanna S.V. and Kamath P.V. (2008) Chromate uptake characteristics of the pristine layered double hydroxides of Mg with Al. *Solid State Sciences*, **10**, 260–266

PT Vale Indonesia Tbk (2017) *Turning Challenges into Opportunities*. Annual Report, PT Vale Indonesia Tbk.

Ravel B. and Newville M. (2005) Athena, artemis, hephaestus: Data analysis for x-ray absorption spectroscopy using ifeffit. *Journal of Synchrotron Radiation*, **12**, 537–541.

Rohatgi A. (2015) *Webplotdigitizer*. https://automeris.io/WebPlotDigitizer

Sanchez-Pastor N., Gigler A.M., Cruz J.A., Park S.H., Jordan G. and Fernandez-Diaz L. (2011) Growth of calcium carbonate in the presence of Cr(VI). *Crystal Growth & Design*, **11**, 3081–3089.

Santos A.L., Dybowska A., Schofield P.F., Herrington R.J., Cibin G. and Johnson D.B. (2022) Chromium (VI) inhibition of low Ph bioleaching of limonitic nickel-cobalt ore. *Frontiers in Microbiology*, 12, https://doi.org/10.3389/fmicb.2021.802991

Schroeder S.L.M., Moggridge G.D., Lambert R.M. and Rayment T. (1997) Thermal dehydration of hydrous chromium hydroxide gel: In situ studies by total electron-yield XAS, *Journal de Physique IV*, **7**(C2), 923–924.

Strunge T., Renforth P. and Van der Spek M. (2022) Towards a business case for CO_2 mineralisation in the cement industry. *Communications Earth & Environment*, **3**, 59

Tang Y., Elzinga E.J., Lee Y.J. and Reeder R.J. (2005) Coprecipitation of chromate with calcite: Batch experiments and spectroscopic study. *Abstracts of Papers of the American Chemical Society*, **230**, U1771-U1771.

Tang Y.Z., Elzinga E.J., Lee Y.J. and Reeder R.J. (2007) Coprecipitation of chromate with calcite: Batch experiments and X-ray absorption spectroscopy. *Geochimica Et Cosmochimica Acta*, **71**, 1480–1493.

Von Euw S., Azais T., Manichev V., Laurent G., Pehau-Arnaudet G., Rivers M., Murali N., Kelly D.J. and Falkowski P.G. (2020) Solid-state phase transformation and self-assembly of amorphous nanoparticles into higher-order mineral structures. *Journal of the American Chemical Society*, **142**, 12811–12825.

Wang F. and Dreisinger D. (2022) Carbon mineralization with concurrent critical metal recovery from olivine. *Proceedings of the National Academy of Sciences of the United States of America*, **119**, e2203937119.

Wang F. and Dreisinger D. (2023) An integrated process of CO_2 mineralization and selective nickel and cobalt recovery from olivine and laterites. *Chemical Engineering Journal*, **451**, 139002.

Wang F., Dreisinger D., Jarvis M., Hitchins T. and Trytten L. (2021) CO_2 mineralization and concurrent utilization for nickel conversion from nickel silicates to nickel sulfides. *Chemical Engineering Journal*, **406**, 126761.

Werner M., Hariharan S.B., Bortolan A.V., Zingaretti D., Baciocchi R. and Mazzotti M. (2013) Carbonation of activated serpentine for direct flue gas mineralization. *Energy Procedia*, **37**, 5929–5937 [*Proceedings of the 11th International Conference on Greenhouse Gas Technologies* (*GHGT*), *Kyoto, JAPAN*, 2012].

World Health Organization. (2020) *Chromium in Drinking-Water. Background Document for Development of Who Guidelines for Drinking-Water Quality*. World Health Organization, Geneva, Switzerland.

Yamamoto G., Kyono A. and Okada S. (2021) Temperature dependence of amorphous magnesium carbonate structure studied by pdf and XAFS analyses. *Scientific Reports*, **11**, 22876.

Zevenhoven R., Kavaliauskaite I. and Denafas G. (2003) An exergy analysis for mineral carbonation. *Proceedings of the 4th International Scientific and Practical Conference on Environment Technology Resources*. Rezekne, Latvia, 2003, pp. 303–308.